Supplementary Information

Regulating Deposition Kinetics *via* A Novel Additive-assisted Chemical Bath Deposition Technology Enables 10.57%-efficient Sb_2Se_3 Solar Cells

Yuqi Zhao[a], Shaoying Wang[a], Chuang Li[a], Bo Che[b, c], Xueling Chen[a], Hongyi Chen[a], Rongfeng Tang[b, c], Xiaomin Wang[d], Guilin Chen[e], Ti Wang[a], Junbo Gong[a], Tao Chen*[b, c], Xudong Xiao*[a], and Jianmin Li*[a]

a. Key Laboratory of Artificial Micro- and Nano-structures of Ministry of Education, and School of Physics and Technology, Wuhan University, Wuhan 430072, China

b. Institute of Energy, Hefei Comprehensive National Science Center, Hefei, China

c. Hefei National Research Centre for Physical Sciences at Microscale, School of Chemistry and Materials Science, University of Science and Technology of China, Hefei 230026, China

d. Center for Biomedical Optics and Photonics (CBOP) & College of Physics and Optoelectronics Engineering, Key Laboratory of Optoelectronic Devices and Systems, Shenzhen University, Shenzhen, 518060, P. R. China

e. College of Physics and Energy, Fujian Normal University, Fuzhou 350007, China

E-mail: tchenmse@ustc.edu.cn, xdxiao@whu.edu.cn, ljmphy@whu.edu.cn

Corresponding authors: Tao Chen (Prof. Chen), Xudong Xiao (Prof. Xiao), Jianmin Li (Dr. Li)

Supplementary Notes

Supplementary Note 1:

The reason for the selection of TU and SU as additives:

As we know, the nucleation and growth of thin films are affected by the solution chemistry condition which can be controlled by the addition of complexing agents in the precursor solution. The choice of appropriate additives plays a crucial role in final films. According to Nieboer and Richardson, by plotting the covalent index $(\chi_m)^2r$ versus ionic index z^2/r metal and metalloid ions can be separated into three groups, that is class A (hard acid), borderline (middle), and class B (soft acid) metal ions.[1, 2] Sb (III) is classified as a borderline metal and thus makes it possible to interact with both soft and hard ligands. A certain number of studies have demonstrated that Sb (III) can be complexed by a large series of oxygen- and sulfur-containing ligands, including TU.[3] On the other hand, the vertical distribution of ions along the covalent index $(\chi_m)^2r$ may be interpreted as a measure of the degree of class B character.[2] Therefore, due to its high $(\chi_m)^2r$, Sb (III) has a high degree of class B character and can be complexed with Selenium-containing ligands. As simple organic compounds, TU and SU have high nucleophilicity caused by the strong electron-donating effect of the amino groups and are known to form stable complexes with metal ions.[4] Based on the above consideration, TU and SU are selected as additives to manipulate the reaction kinetics in this work.

Supplementary Note 2:

Reaction equations during the CBD process:

(i) $KSbC_4H_4O_7 \cdot 0.5H_2O$ in deionized water

First, $KSbC_4H_4O_7 \cdot 0.5H_2O$ hydrolyzes in deionized water to produce $(SbO)^+$ ions

$$KSbC_4H_4O_7 \cdot 0.5H_2O \leftrightharpoons K^+ + (SbO)^+ + C_4O_4O_6^{2-} + 0.5H_2O \quad (1)$$

(ii) The reaction of $(SbO)^+$

With the addition of SSS, a vast amount of antimony hydroxide SbO(OH) (or $Sb(OH)_3$) produces

$$(SbO)^+ + OH^- \rightarrow (SbO)OH\downarrow \quad (2)$$

Meanwhile, under alkaline conditions, $(SbO)^+$ reacts with Se precursors to form Sb_2Se_3

$$2(SbO)^+ + 3Se_2SO_3^{2-} + 2OH^- \rightarrow Sb_2Se_3\downarrow + 3SO_4^{2-} + H_2O \quad (3)$$

(iii) Addition of TU and SU

$$(SbO)^+ + n\,(N_2H_4CS) + OH^- \leftrightharpoons [(SbO)OH(N_2H_4CS)_n] \quad (4)$$

$$(SbO)^+ + n\,(N_2H_4CSe) + OH^- \leftrightharpoons [(SbO)OH(N_2H_4CSe)_n] \quad (5)$$

$$N_2H_4CSe + OH^- \leftrightharpoons HSe^- + NCNH_2 \quad (6)$$

$$2(SbO)^+ + 3HSe^- + H^+ \rightarrow Sb_2Se_3\downarrow + 2H_2O \quad (7)$$

Supplementary Note 3

Considering the slight difference in band gaps between the Sb_2Se_3 films, we calculated the voltage deficit as $V_{OC\text{-}def} = V_{OC}^{SQ} - V_{OC}$, which facilitates the comparison of different materials and band gaps. The maximum theoretical (V_{OC}^{SQ}) can be calculated as V_{OC}^{SQ} (V) = 0.932*E_g (eV) - 0.167. To minimize the error, the mean values of the box statistics of V_{OC} in Figure 3b acted as the actual V_{OC}, in which Control-Sb_2Se_3, TU-Sb_2Se_3, and SU-Sb_2Se_3 are 0.393V, 0.447V and 0.459V, respectively. By calculation, the $V_{OC\text{-}def}$ of the three devices is 0.623V, 0.532V, and 0.492V, respectively, suggesting the lowest $V_{OC\text{-}def}$ in SU-Sb_2Se_3 devices. According to the literature[5], the Urbach energy (E_U) demonstrates a close relation with $V_{OC\text{-}def}$, implying that E_U can be used as another metric to evaluate the V_{OC}. Compared with TU-Sb_2Se_3 device, the lower E_U value indicates a lower voltage deficit in SU-Sb_2Se_3 device, which agree with the calculated results of $V_{OC\text{-}def}$.

Supplementary Note 4

The diode parameters were derived from the dark J–V curves of Sb_2Se_3 solar cells through the single exponential diode equation (8):

$$J = J_0 exp\left[\frac{AKT}{q}(V - R_S J)\right] + G_{SH}V - J_L \quad (8)$$

where K is the Boltzmann constant, T is the temperature in actual condition, q is the quantity of electric charge, G_{SH} is the shun conduction, A is the diode ideality factor, R_S is the series resistance, and J_0 is the reverse saturation current density.

(1) First, the derivative dJ/dV against V (Figure 4b) is plotted, where the value in the flat range under reverse bias is equal to G.

(2) Then, we need to plot the dV/dJ to $(J + J_{SC})^{-1}$. A correction can be made for the case in which G is not negligible by plotting $(J + J_{SC}\text{-}GV)^{-1}$ using the value of G obtained from Figure 4b, as shown in Figure 4c. A linear fit to the data gives an intercept of R and a slope AkT/q from which A can be calculated.

(3) Finally, the $\ln(J + J_{SC} – GV)$ against V-RJ can be plotted using the value of R and G, as shown in Figure 4d. The linear region in current can be used to fit the diode equation, where the intercept of the fitting line gives J_0 and the slope equals q/AkT.

Supplementary Figures

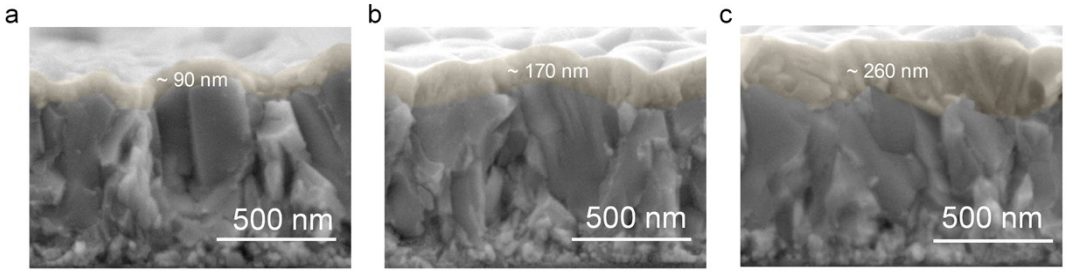

Figure S1 The cross-sectional SEM images of (a) Control-Sb_2Se_3 film, (b) TU-Sb_2Se_3 film, and (c) SU-Sb_2Se_3 film deposited at 95℃ for 2h by CBD method.

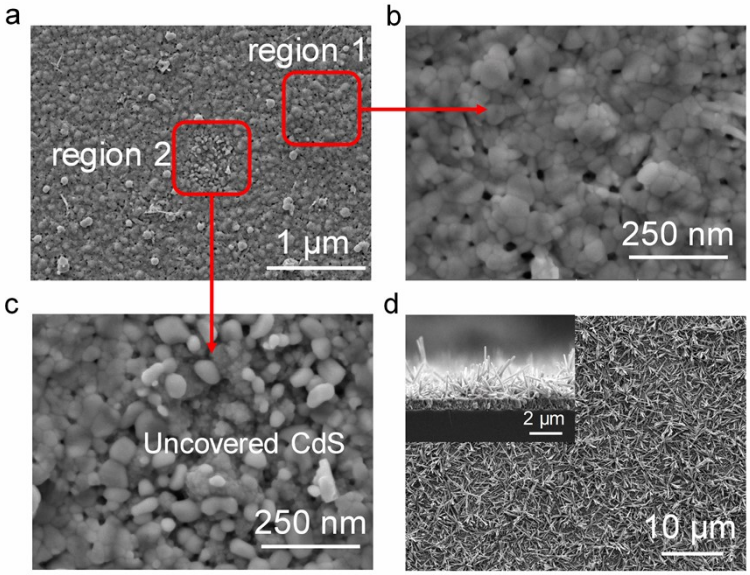

Figure S2 The surface SEM images of (a) the Control-Sb_2Se_3 film, (b) the zoomed region 1 of Control-Sb_2Se_3 film, and (c) the zoomed region 2 of Control-Sb_2Se_3 film. The Control-Sb_2Se_3 film was inhomogeneous and did not completely cover the CdS substrate. (d) The surface SEM images of Control-Sb_2Se_3 film with deposited at 95℃ for 6h. The inset shows the corresponding cross-sectional SEM image.

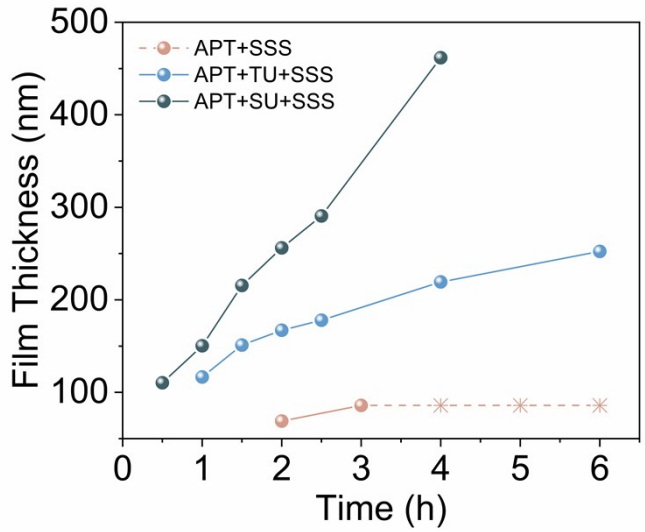

Figure S3 Relationships between the film thickness and deposition time.

Note for the Control-Sb_2Se_3 film thickness curve with time: the Control-Sb_2Se_3 film exhibited highly dispersed and porous rod-like structures after the growth for more than 4 h (Figure S2d), where the thickness cannot be determined. Hence, the relationship curve between the film thickness and deposition time is shown as a dotted line after 4h.

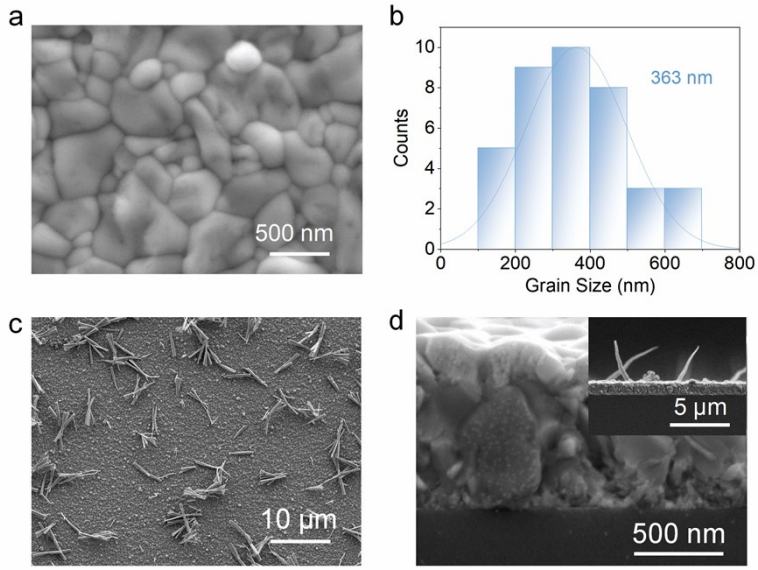

Figure S4 (a, c, d) The surface SEM images of TU-Sb_2Se_3 film deposited at 95℃ for 6h. Inset in (d) shows the corresponding cross-sectional SEM image. (b) Grain size distribution histogram of the TU-Sb_2Se_3 films deposited for 6h.

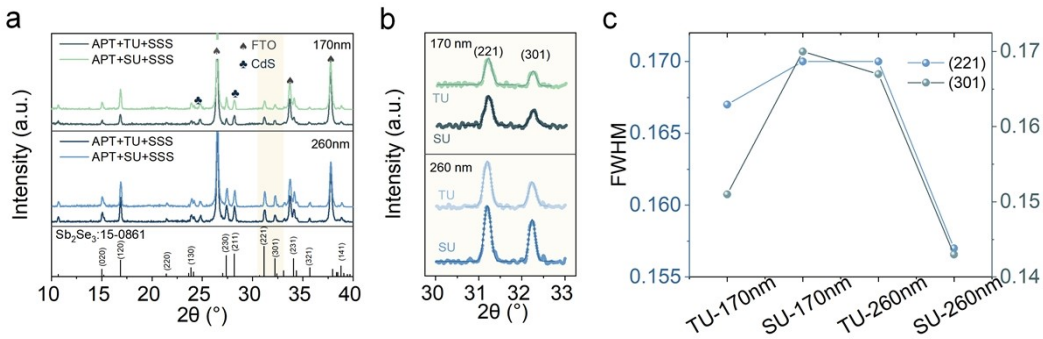

Figure S5 (a) X-ray diffraction patterns and (b) enlarged XRD patterns of the TU-Sb_2Se_3 and SU-Sb_2Se_3 samples.

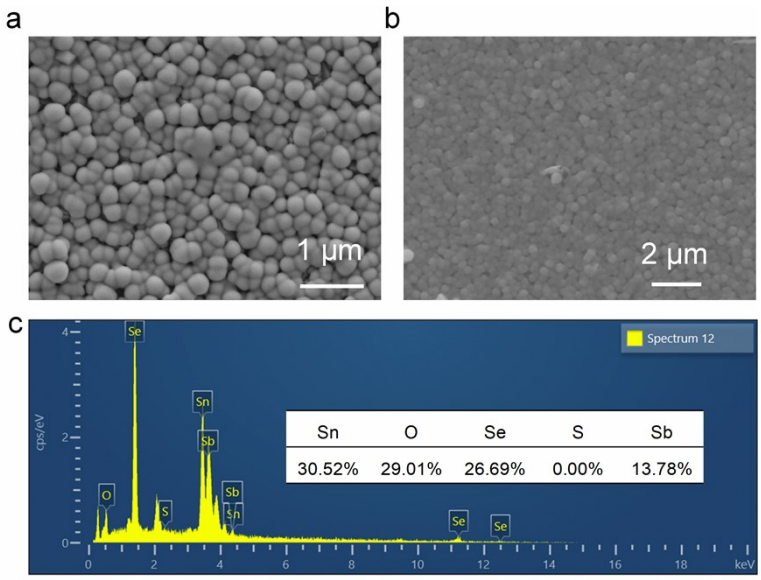

Figure S6 (a-b) Surface SEM images and (c) EDS spectrum of the TU-Sb_2Se_3 film.

Note: The TU-Sb_2Se_3 film was obtained by directly depositing on the cleaned FTO-glass at 95°C for 6h.

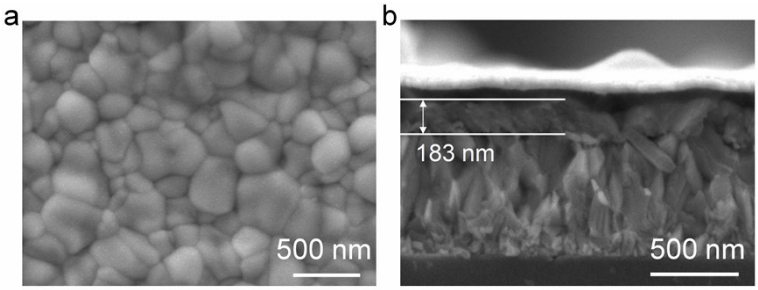

Figure S7 (a) Surface and (b) cross-sectional SEM image of TU+SU-Sb_2Se_3 film deposited at 95°C for 2h.

Note: To probe the function of SU in the CBD synthesis, films fabricated with both TU and SU were also investigated. SEM images show that a thicker Sb_2Se_3 film in comparison with the TU-only film was obtained, indicating that a certain amount of SU was probably involved in the reaction.

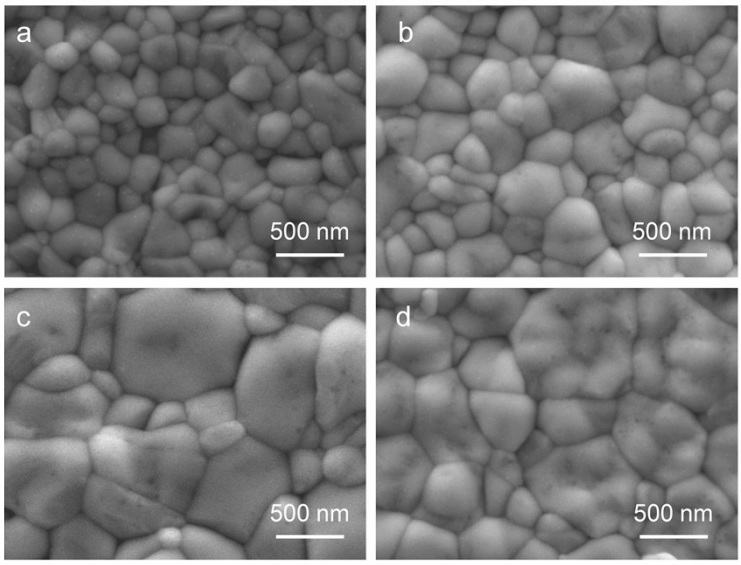

Figure S8 Surface morphology of Sb_2Se_3 films with the addition of (a) 5mg, (b) 20mg, (c) 50mg, and (d)100mg SU.

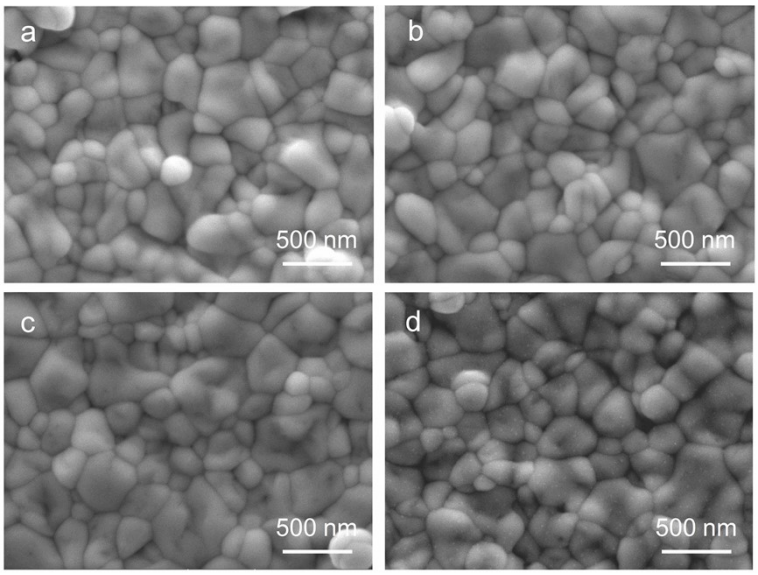

Figure S9 Surface morphology of Sb_2Se_3 films with the addition of (a) 0.2g, (b) 0.4g, (c) 0.6g, and (d) 0.8g TU.

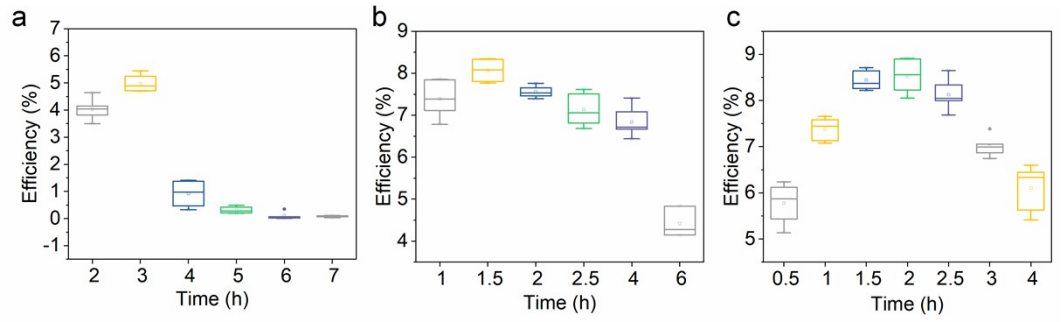

Figure S10 Statistical boxplot of conversion efficiency (%) for the (a) Control-Sb_2Se_3 solar cell, (b) TU-Sb_2Se_3 solar cell, and (c) SU-Sb_2Se_3 solar cell as a function of deposited time.

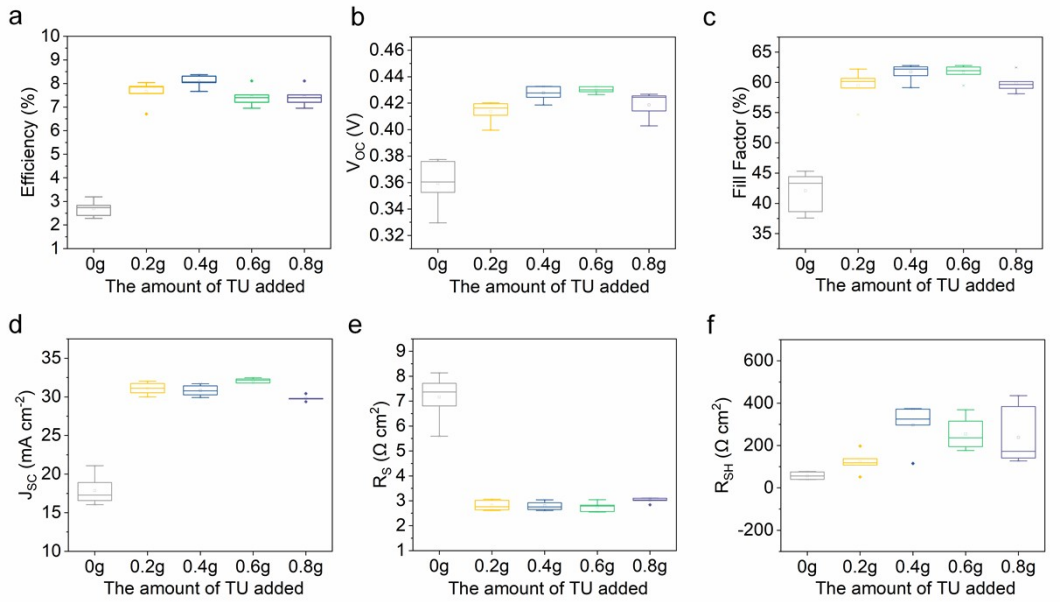

Figure S11 Statistical boxplots of (a) conversion efficiency, (b) V_{OC} (V), (c) J_{SC} (mA cm^{-2}), (d) Fill factors (%), (e) R_S (Ω cm^2), and (f) R_{SH} (Ω cm^2) as a function of the amount of TU added for the TU-Sb_2Se_3 solar cells.

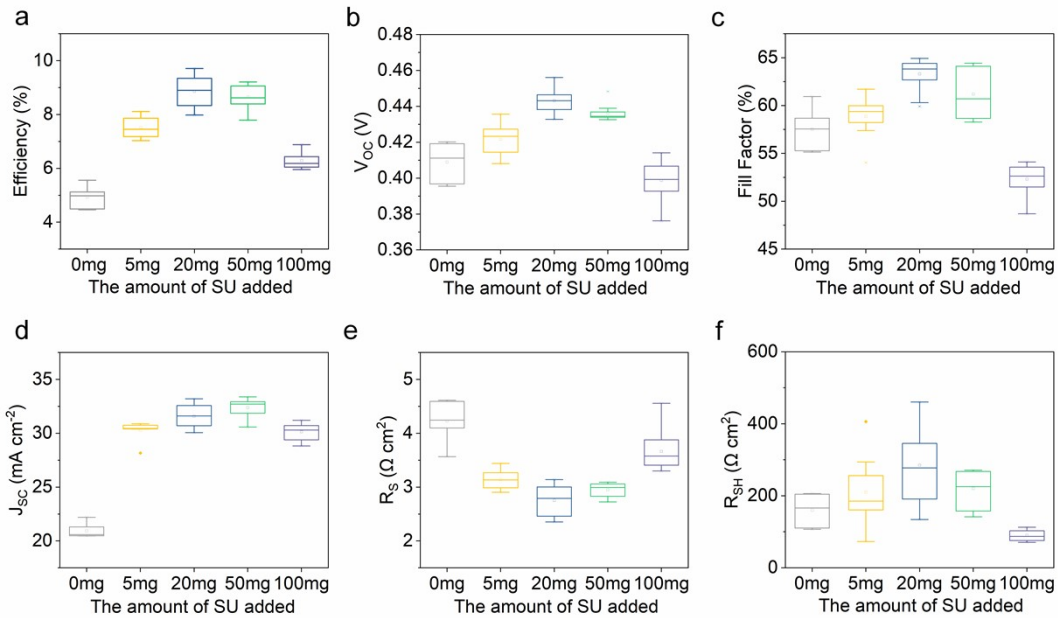

Figure S12 Statistical boxplots of (a) conversion efficiency, (b) V_{OC} (V), (c) J_{SC} (mA cm^{-2}), (d) Fill factors (%), (e) R_S (Ω cm^2), and (f) R_{SH} (Ω cm^2) as a function of the amount of SU added for the SU-Sb_2Se_3 solar cells.

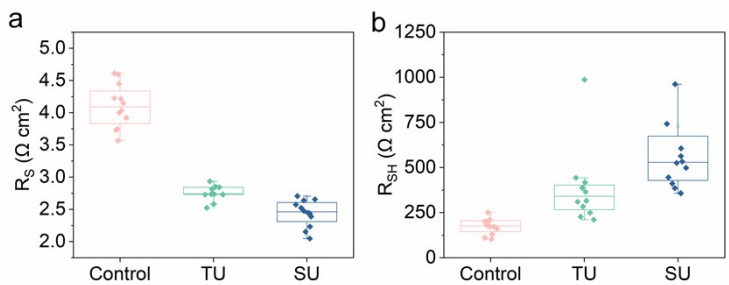

Figure S13 Statistical boxplots of (a) R_S (Ω cm^2) and (b) R_{SH} (Ω cm^2) for the Control-Sb_2Se_3, TU-Sb_2Se_3, and SU-Sb_2Se_3 solar cells.

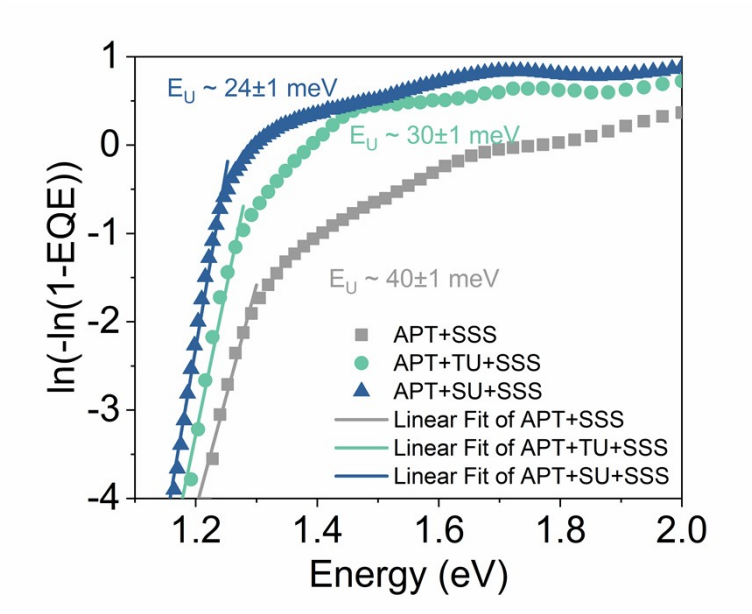

Figure S14 The Urbach energy calculated from the EQE data of devices.

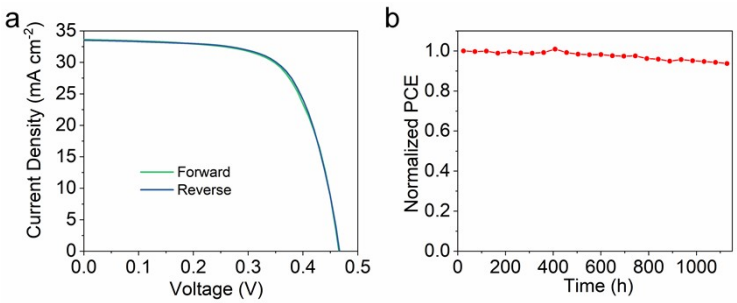

Figure S15 (a) The scan-direction-dependence of the J-V curves and (b) the stabilities of SU-Sb_2Se_3 solar cell.

Note: Without encapsulation, we tested the stability of SU-Sb_2Se_3 solar cell housed in a dry cabinet at 20% ± 5% relative humidity and ambient temperature. After 1000 hours of storage, the SU-Sb_2Se_3 solar cell retains over 93% of the initial PCE.

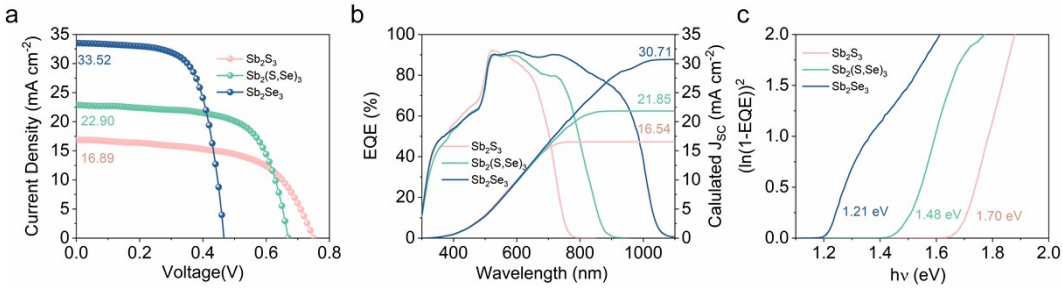

Figure S16 (a) The J-V curves, (b) EQE spectra, and (c) The bandgap calculated from EQE spectra for the Sb_2S_3, $Sb_2(S,Se)_3$, and Sb_2Se_3 solar cells, respectively.

Note: The ΔJ_{SC} between the Jsc obtained by J-V curves and EQE spectra are 0.35, 1.05, and 2.81 mA cm^{-2} for the Sb_2S_3 (1.7 eV), $Sb_2(S,Se)_3$ (1.48 eV), and Sb_2Se_3 (1.21 eV) solar cells, respectively. It can be found that the values of ΔJ_{SC} are correlated with the elemental composition. Interestingly, the J_{SC} calculated by EQE spectrum agrees well with the J_{SC} obtained from the corresponding J-V curves of the S-rich sample. In contrast, as for Se-rich sample, this mismatching of J_{SC} among EQE curves and J-V curves became apparent.

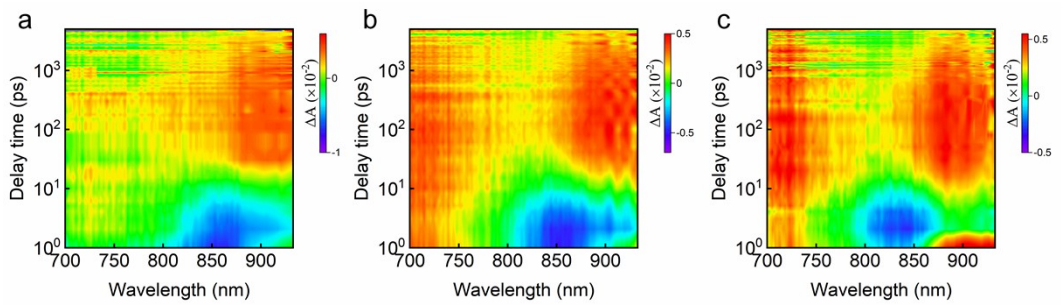

Figure S17 Pseudo-color plot of TAS of (a) Control-Sb_2Se_3 film, (b) TU-Sb_2Se_3 film, and (c) SU-Sb_2Se_3 film deposited on FTO/CdS at the excitation of 400nm laser pulse.

Note on the femtosecond-TA measurement: The transient dynamics are extracted from pseudo-color TAS and fitted by the bi-exponential equation (9) [6]

$$y = A_1 e^{(-\frac{x}{\tau_1})} + A_2 e^{(-\frac{x}{\tau_2})} \tag{9}$$

The average lifetime τ_{ave} was estimated from the fitting parameters according to the following equation (10)

$$\tau_{ave} = \frac{\sum A_i \tau_i^2}{\sum A_i \tau_i} \tag{10}$$

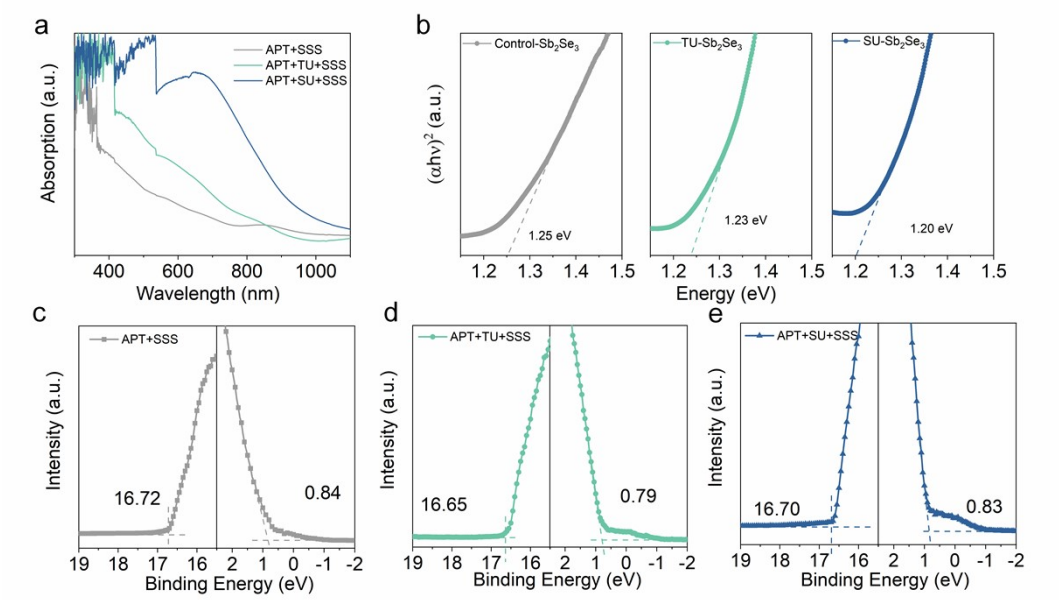

Figure S18 (a) UV-vis absorption spectra and (b) Tauc plots obtained from absorption spectra. (c-e) Energy positions of secondary electron cut-offs and valence band edge estimated from the UPS spectra.

Table S1. Recipes of Sb_2Se_3 deposited by CBD method.

Samples	$[Sb^{3+}]$ [a]	Additives	$[Se^{2-}]$ [b]	Deposition Temp.	Deposition time
APT+SSS	1.5mmol	---	0.2mmol	95℃	120-420min
APT+TU+SSS	1.5mmol	5.25mmol	0.2mmol	95℃	60-360min
APT+SU+SSS	1.5mmol	0.16mmol	0.2mmol	95℃	90-240min

[a]$KSbC_4H_4O_7 \cdot 0.5H_2O$, antimony potassium tartrate

[b]$Na_2Se_2SO_3$, Sodium selenosulfate

Table S2. The FWHM of the (221) and (301) peaks of Control-Sb_2Se_3 film, TU-Sb_2Se_3 film, and SU-Sb_2Se_3 film obtained by Gaussian fittings.

Samples	FWHM - (221)	FWHM - (301)
APT+SSS-90 nm	0.184	0.157
APT+TU+SSS-170 nm	0.167	0.151
APT+SU+SSS-170 nm	0.170	0.170
APT+TU+SSS-260nm	0.170	0.167
APT+SU+SSS-260 nm	0.157	0.143

Table S3. The XPS results of Control-Sb_2Se_3 film, TU-Sb_2Se_3 film, and SU-Sb_2Se_3 film.

Samples	Chemical bond	Peak		Area (P) CPS.eV	
		$3d_{5/2}$	$3d_{3/2}$	$3d_{5/2}$	$3d_{3/2}$
APT+SSS	Sb-Se	528.66	538.07	3.12E5	2.27E5
	Sb-O	530.03	539.36	4.17E4	1.50E4
APT+TU+SSS	Sb-Se	528.79	538.10	5.70E5	3.54E5
	Sb-O	530.49	539.64	1.59E4	5.46E3
APT+SU+SSS	Sb-Se	528.72	538.07	5.95E5	3.67E5
	Sb-O	530.30	539.58	1.31E4	2.42E3

Table S4. The summary of photovoltaic parameters of Sb_2Se_3 devices prepared *via* different methods.

Methods	Device structure	V_{OC} (V)	PCE (%)	FF (%)	J_{SC} (mA cm^{-2})	Year	Ref.
TE[a]	FTO/CdS/Sb_2Se_3/Au	0.300	1.9	48.0	13.2	2014	7
	FTO/Sb_2Se_3/CdS/ZnO/ZnO:Al/Au	0.354	2.1	33.5	17.84	2014	8
	ITO/CdS/Sb_2Se_3/Au	0.360	4.8	52.5	25.3	2015	9
Co-eva[b]	FTO/CdS/Sb_2Se_3/Au	0.364	3.47	41.26	23.14	2016	10
	Mo/Sb_2Se_3/CdS/ZnO/ITO/Ag	0.427	4.25	58.15	17.11	2017	11
	Mo/Sb_2Se_3/CdS/ZnO/AZO/Au	0.376	4.51	47.24	25.39	2019	12
RTE[c]	FTO/CdS/Sb_2Se_3/Au	0.400	5.6	55.7	25.1	2015	13
	FTO/ZnO/Sb_2Se_3/Au	0.391	5.93	57.8	26.2	2017	14
	ITO/CdS/Sb_2Se_3/PbS CQD/Au	0.427	6.5	59.3	25.5	2017	15
	FTO/TiO_2/Sb_2Se_3/Au	0.358	5.6	55.1	28.3	2017	16
VTD[d]	ITO/CdS/Sb_2Se_3/Au	0.420	7.6	60.40	29.90	2018	17
	ITO/CdS/Sb_2Se_3/CuSCN/Au	0.423	7.4	57.0	30.8	2018	18
	ITO/SnO_2/CdS/Sb_2Se_3/Au	0.431	7.5	63.2	27.6	2019	19
	FTO/CdS/Sb_2Se_3/Al_2O_3/Au	0.405	7.35	58.52	31.02	2020	20
	ITO/CdS/Sb_2Se_3/C/Ag	0.412	6.09	53.6	27.8	2021	21
	Mo/Sb_2Se_3/CdS/ITO/Ag	0.513	7.40	58.74	24.74	2022	22
CSS[e]	FTO/CdS/Sb_2Se_3/Graphite	0.421	4.27	46.65	21.74	2018	23
	FTO/CdS/Sb_2Se_3/CZ-TA/Au	0.421	6.84	57.1	28.4	2018	24
	Mo/Sb_2Se_3/CdZnS/ZnO/AZO	0.403	6.71	64.78	25.69	2019	25
	Mo/$MoSe_2$/ Sb_2Se_3/TiO_2/CdS/ZnO/AZO	0.400	9.2	70.3	32.58	2019	26
	FTO/CdS/Sb_2Se_3/t-Se/Au	0.413	7.45	62.3	28.9	2020	27
	Mo/Sb_2Se_3/CdS/IZO/AZO/Ag	0.446	6.43	54.9	26.4	2021	28
	Mo/Sb_2Se_3/CdS/i-ZnO/AZO/Ag	0.505	8.5	60.7	27.74	2021	29
IVD[f]	Mo/$MoSe_2$/Sb_2Se_3/CdS/i-ZnO/AZO	0.488	10.12	67.19	30.86	2022	30

MSD[g]	Mo/Sb_2Se_3/CdS/ZnO/AZO/Ag	0.437	3.35	48.0	15.93	2018	31
	Mo/Sb_2Se_3/CdS/ITO/Ag	0.494	6.06	47.7	25.91	2019	32
	FTO/CdS/Sb_2Se_3/Au	0.350	3.47	51.6	19.2	2019	33
	Mo/Sb_2Se_3/CdS/ITO/Ag	0.504	6.84	54.47	24.91	2020	34
	Mo/Sb_2Se_3/CdS/ITO/Ag	0.520	8.64	59.8	27.8	2022	5
PLD[h]	FTO/CdS/Sb_2Se_3/Au	0.328	4.41	46.40	28.87	2020	35
	FTO/SnO_2/CdS/Sb_2Se_3/Au	0.334	4.77	45.04	31.68	2020	36
LT-PED[i]	FTO/Sb_2Se_3/CdS/ZnO/AZO	0.260	3.1	40.2	29.60	2020	37
Spin-coating	FTO/mp-TiO_2/Sb_2Se_3/HTM/Au	0.304	3.21	47.2	22.3	2013	38
	FTO/TiO_2/Sb_2Se_3/Au	0.520	2.26	42.3	10.3	2014	39
	FTO/TiO_2/CdS/Sb_2Se_3/Spiro-OMeTAD/Au	0.340	3.9	41.9	27.2	2019	40
	FTO/CdS/Sb_2Se_3/Spiro-OMeTAD/Au	0.360	5.4	51.5	29.0	2020	41
ED[j]	FTO/TiO_2(compact)/Sb_2Se_3/CuSCN/Au	0.302	2.1	38.3	18.0	2014	42
HD[k]	FTO/CdS/Sb_2Se_3/Spiro-OMeTAD/Au	0.449	7.89	62.1	28.3	2021	43
CBD[l]	TCO/CdS/Sb_2Se_3:Sb_2O_2/PbS/C/Ag	0.540	0.13	37.0	0.67	2009	44
	FTO/CdS/Sb_2Se_3/Spiro-OMeTAD/Au	0.467	10.57	67.64	33.52	2022	This work

[a]thermal evaporation

[b]co-evaporation

[c]rapid thermal evaporation

[d]vapor transport deposition

[e]close-spaced sublimation

[f]injection vapor deposition

[g]magnetron sputtering deposition

[h]pulsed laser deposition

[i]low-temperature pulsed electron deposition

[j]electrodeposition

[k]hydrothermal deposition

[l]chemical bath deposition

Table S5. Electrical property parameters of Control-Sb_2Se_3 solar cell, TU-Sb_2Se_3 solar cell, and SU-Sb_2Se_3 solar cell.

Samples	G (mS cm^{-2})	R (Ω cm^2)	A	J_0 (mA cm^{-2})
APT+SSS	0.718	11.35	2.22	1.73×10^{-3}
APT+TU+SSS	0.337	5.43	1.81	1.00×10^{-3}
APT+SU+SSS	0.062	1.36	1.62	6.83×10^{-4}

Table S6. Carrier lifetimes obtained from TAS decay kinetics at 906 nm curves for Control-Sb_2Se_3, TU-Sb_2Se_3, and SU-Sb_2Se_3 films. The measured Sb_2Se_3 films were deposited on FTO/CdS.

Samples	A_1	τ_1	A_2	τ_2	τ_{av}
APT+SSS	0.144	80.78	0.727	2043.62	2028.37
APT+TU+SSS	0.116	45.75	0.741	3214.51	3207.47
APT+SU+SSS	0.093	22.88	0.814	6552.12	6549.52

Table S7. Band gap (E_g), Fermi level (E_F), conduction band (E_{CB}) and valence band (E_V) positions of the Control-Sb_2Se_3, TU-Sb_2Se_3, and SU-Sb_2Se_3 films.

Samples	E_F (eV)	E_{CB} (eV)	E_{VB} (eV)	E_g (eV)
APT+SSS	4.48	4.07	5.32	1.25
APT+TU+SSS	4.55	4.11	5.34	1.23
APT+SU+SSS	4.50	4.13	5.33	1.20

Table S8. EDS results of the Control-Sb_2Se_3, TU-Sb_2Se_3, and SU-Sb_2Se_3 films.

Samples	O	Sb	Se	Sn	Se/Sb
APT+SSS	47.00	3.43	7.34	42.23	2.14
APT+TU+SSS	27.31	9.83	21.09	41.77	2.15
APT+SU+SSS	17.85	20.31	38.54	23.30	1.90

References:

1. E. Nieboer and D. H. Richardson, *Environmental Pollution Series B, Chemical and Physical*, 1980, **1**, 3-26.
2. E. Nieboer, G. G. Fletcher and Y. Thomassen, *Journal of Environmental Monitoring*, 1999, **1**, 1-14.
3. M. Filella, N. Belzile and Y.-W. Chen, *Earth-Science Reviews*, 2002, **59**, 265-285.
4. S. Ahmad and A. A. Isab, *Transition Metal Chemistry*, 2003, **28**, 540-543.
5. R. Tang, S. Chen, Z. H. Zheng, Z. H. Su, J. T. Luo, P. Fan, X. H. Zhang, J. Tang and G. X. Liang, *Adv Mater*, 2022, **34**, e2109078.
6. J. A. Christians, D. T. Leighton and P. V. Kamat, *Energy Environ. Sci.*, 2014, **7**, 1148-1158.
7. M. Luo, M. Leng, X. Liu, J. Chen, C. Chen, S. Qin and J. Tang, *Applied Physics Letters*, 2014, **104**, 173904.
8. X. Liu, J. Chen, M. Luo, M. Leng, Z. Xia, Y. Zhou, S. Qin, D. J. Xue, L. Lv, H. Huang, D. Niu and J. Tang, *ACS Appl Mater Interfaces*, 2014, **6**, 10687-10695.
9. X. Liu, C. Chen, L. Wang, J. Zhong, M. Luo, J. Chen, D.-J. Xue, D. Li, Y. Zhou and J. Tang, *Progress in Photovoltaics: Research and Applications*, 2015, **23**, 1828-1836.
10. Z. Li, H. Zhu, Y. Guo, X. Niu, X. Chen, C. Zhang, W. Zhang, X. Liang, D. Zhou, J. Chen and Y. Mai, *Applied Physics Express*, 2016, **9**, 052302.
11. Z. Li, X. Chen, H. Zhu, J. Chen, Y. Guo, C. Zhang, W. Zhang, X. Niu and Y. Mai, *Solar Energy Materials and Solar Cells*, 2017, **161**, 190-196.
12. S.-N. Park, S.-Y. Kim, S.-J. Lee, S.-J. Sung, K.-J. Yang, J.-K. Kang and D.-H. Kim, *Journal of Materials Chemistry A*, 2019, **7**, 25900-25907.
13. Y. Zhou, L. Wang, S. Chen, S. Qin, X. Liu, J. Chen, D.-J. Xue, M. Luo, Y. Cao, Y. Cheng, E. H. Sargent and J. Tang, *Nature Photonics*, 2015, **9**, 409-415.
14. L. Wang, D.-B. Li, K. Li, C. Chen, H.-X. Deng, L. Gao, Y. Zhao, F. Jiang, L. Li, F. Huang, Y. He, H. Song, G. Niu and J. Tang, *Nature Energy*, 2017, **2**, 17046.
15. C. Chen, L. Wang, L. Gao, D. Nam, D. Li, K. Li, Y. Zhao, C. Ge, H. Cheong, H. Liu, H. Song and J. Tang, *ACS Energy Letters*, 2017, **2**, 2125-2132.
16. C. Chen, Y. Zhao, S. Lu, K. Li, Y. Li, B. Yang, W. Chen, L. Wang, D. Li, H. Deng, F. Yi and J. Tang, *Advanced Energy Materials*, 2017, **7**, 1700866.
17. X. Wen, C. Chen, S. Lu, K. Li, R. Kondrotas, Y. Zhao, W. Chen, L. Gao, C. Wang, J. Zhang, G. Niu and J. Tang, *Nat Commun*, 2018, **9**, 2179.
18. K. Li, S. Wang, C. Chen, R. Kondrotas, M. Hu, S. Lu, C. Wang, W. Chen and J. Tang, *Journal of Materials Chemistry A*, 2019, **7**, 9665-9672.
19. J. Tao, X. Hu, Y. Guo, J. Hong, K. Li, J. Jiang, S. Chen, C. Jing, F. Yue, P. Yang, C. Zhang, Z. Wu, J. Tang and J. Chu, *Nano Energy*, 2019, **60**, 802-809.
20. H. Guo, X. Jia, S. H. Hadke, J. Zhang, W. Wang, C. Ma, J. Qiu, N. Yuan, L. H. Wong and J. Ding, *Journal of Materials Chemistry C*, 2020, **8**, 17194-17201.
21. W. Wang, Z. Cao, L. Wu, F. Liu, J. Ao and Y. Zhang, *ACS Applied Energy Materials*, 2021, **4**, 13335-13346.
22. G. Liang, M. Chen, M. Ishaq, X. Li, R. Tang, Z. Zheng, Z. Su, P. Fan, X. Zhang and S. Chen, *Adv Sci (Weinh)*, 2022, **9**, e2105142.
23. L. Guo, B. Zhang, Y. Qin, D. Li, L. Li, X. Qian and F. Yan, *Solar RRL*, 2018, **2**, 1800128.

24. D.-B. Li, X. Yin, C. R. Grice, L. Guan, Z. Song, C. Wang, C. Chen, K. Li, A. J. Cimaroli, R. A. Awni, D. Zhao, H. Song, W. Tang, Y. Yan and J. Tang, *Nano Energy*, 2018, **49**, 346-353.
25. G. Li, Z. Li, X. Liang, C. Guo, K. Shen and Y. Mai, *ACS Appl Mater Interfaces*, 2019, **11**, 828-834.
26. Z. Li, X. Liang, G. Li, H. Liu, H. Zhang, J. Guo, J. Chen, K. Shen, X. San, W. Yu, R. E. I. Schropp and Y. Mai, *Nat Commun*, 2019, **10**, 125.
27. K. Shen, Y. Zhang, X. Wang, C. Ou, F. Guo, H. Zhu, C. Liu, Y. Gao, R. E. I. Schropp, Z. Li, X. Liu and Y. Mai, *Adv Sci (Weinh)*, 2020, **7**, 2001013.
28. S. Rijal, D.-B. Li, R. A. Awni, S. S. Bista, Z. Song and Y. Yan, *ACS Applied Energy Materials*, 2021, **4**, 4313-4318.
29. S. Rijal, D. B. Li, R. A. Awni, C. Xiao, S. S. Bista, M. K. Jamarkattel, M. J. Heben, C. S. Jiang, M. Al‐Jassim, Z. Song and Y. Yan, *Advanced Functional Materials*, 2021, **32**, 2110032.
30. Z. Duan, X. Liang, Y. Feng, H. Ma, B. Liang, Y. Wang, S. Luo, S. Wang, R. E. I. Schropp, Y. Mai and Z. Li, *Advanced Materials*, 2022, **34**, 2202969.
31. G.-X. Liang, Z.-H. Zheng, P. Fan, J.-T. Luo, J.-G. Hu, X.-H. Zhang, H.-L. Ma, B. Fan, Z.-K. Luo and D.-P. Zhang, *Solar Energy Materials and Solar Cells*, 2018, **174**, 263-270.
32. R. Tang, Z.-H. Zheng, Z.-H. Su, X.-J. Li, Y.-D. Wei, X.-H. Zhang, Y.-Q. Fu, J.-T. Luo, P. Fan and G.-X. Liang, *Nano Energy*, 2019, **64**, 103929.
33. C. Ma, H. Guo, X. Wang, Z. Chen, Q. Cang, X. Jia, Y. Li, N. Yuan and J. Ding, *Solar Energy*, 2019, **193**, 275-282.
34. G.-X. Liang, Y.-D. Luo, S. Chen, R. Tang, Z.-H. Zheng, X.-J. Li, X.-S. Liu, Y.-K. Liu, Y.-F. Li, X.-Y. Chen, Z.-H. Su, X.-H. Zhang, H.-L. Ma and P. Fan, *Nano Energy*, 2020, **73**, 104806.
35. K. Yang, B. Li and G. Zeng, *Solar Energy Materials and Solar Cells*, 2020, **208**, 110381.
36. K. Yang, B. Li and G. Zeng, *Journal of Alloys and Compounds*, 2020, **821**, 153505.
37. F. Pattini, S. Rampino, F. Mezzadri, D. Calestani, G. Spaggiari, M. Sidoli, D. Delmonte, A. Sala, E. Gilioli and M. Mazzer, *Solar Energy Materials and Solar Cells*, 2020, **218**, 110724.
38. Y. C. Choi, T. N. Mandal, W. S. Yang, Y. H. Lee, S. H. Im, J. H. Noh and S. I. Seok, *Angew Chem Int Ed Engl*, 2014, **53**, 1329-1333.
39. Y. Zhou, M. Leng, Z. Xia, J. Zhong, H. Song, X. Liu, B. Yang, J. Zhang, J. Chen, K. Zhou, J. Han, Y. Cheng and J. Tang, *Advanced Energy Materials*, 2014, **4**, 1301846.
40. X. Wang, R. Tang, Y. Yin, H. Ju, S. a. Li, C. Zhu and T. Chen, *Solar Energy Materials and Solar Cells*, 2019, **189**, 5-10.
41. Y. Ma, B. Tang, W. Lian, C. Wu, X. Wang, H. Ju, C. Zhu, F. Fan and T. Chen, *Journal of Materials Chemistry A*, 2020, **8**, 6510-6516.
42. T. T. Ngo, S. Chavhan, I. Kosta, O. Miguel, H. J. Grande and R. Tena-Zaera, *ACS Appl Mater Interfaces*, 2014, **6**, 2836-2841.
43. D. Liu, R. Tang, Y. Ma, C. Jiang, W. Lian, G. Li, W. Han, C. Zhu and T. Chen, *ACS Appl Mater Interfaces*, 2021, **13**, 18856-18864.
44. S. Messina, M. T. S. Nair and P. K. Nair, *Journal of The Electrochemical Society*, 2009, **156**, H327.